L. Kang[1], R. T. Marchand [1], R. Wood [1], and I. L. McCoy[2,3]

[1] Department of Atmospheric Sciences, University of Washington, Seattle, Washington, USA

[2] Rosenstiel School of Marine and Atmospheric Sciences, University of Miami, Miami, Florida, USA

[3] University Corporation for Atmospheric Research, Boulder, CO, USA

Corresponding author: Litai Kang (kanglt@uw.edu)

†Additional author notes should be indicated with symbols (current addresses, for example).

Key Points:

- A simple source-and-sink budget model accurately predicts *in situ* observations of Southern Ocean cloud droplet number concentration.
- Coalescence scavenging by liquid droplets is a dominant sink of Southern Ocean cloud condensation nuclei.
- Free tropospheric aerosol more strongly controls cloud droplet number concentration than surface aerosol during austral summer.

Abstract

Cloud droplet number concentration (N_d) is a key microphysical property that is largely controlled by the balance between sources and sinks of aerosols that serve as cloud condensation nuclei (CCN). Despite being a key sink of CCN, the impact of coalescence scavenging on Southern Ocean (SO) cloud is poorly known. We apply a simple source-and-sink budget model based on parameterizations to austral summer aircraft observations to test model behavior and examine the relative influence of processes that determine N_d in SO stratocumulus clouds. The model predicts N_d with little bias and a correlation coefficient of ~0.7 compared with observations. Coalescence scavenging is found to be an important sink of CCN in both liquid and mixed-phase precipitating stratocumulus and reduces the predicted N_d by as much as 90% depending on the precipitation rate. The free tropospheric aerosol source controls N_d more strongly than the surface aerosol source during austral summer.

Plain Language Summary

Low altitude stratiform clouds are ubiquitous over the Southern Ocean (SO) and have a profound climate impact through reflecting sunlight back to space, cooling the earth. The number of water droplets in a given volume (the concentration) is a key variable that determines the reflective ability of the cloud. The cloud droplet number concentration is largely set by the number of aerosols (tiny airborne particles) on which water can condense and is controlled by the balance between sources that generate aerosols (e.g., ocean biology, sea spray) and sinks which remove aerosols from the atmosphere. The formation of liquid precipitation in clouds (drizzle) is a strong sink of aerosols because each precipitation droplet is created through the merger of many cloud droplets (i.e., coalescence) where each cloud droplet contains at least one aerosol particle. Here, we test a simple source-and-sink model to predict SO cloud droplet number concentrations using aircraft measurements from a recent aircraft campaign in the SO during austral summer. We find this model can predict cloud droplet number well and that liquid precipitation processes are important in controlling droplet number concentration (and thus cloud reflectance) over the SO.

1 Introduction

Low altitude stratiform clouds are ubiquitous over the Southern Ocean (SO) (Mace et al., 2009, 2010, 2020; Huang et al., 2016). These clouds are crucial to climate because they reflect shortwave radiation back to space, cooling the planet, locally reducing ocean heat uptake (Sallée et al., 2013; Schneider & Reusch, 2016), and profoundly affecting the global atmospheric circulation (Hwang and Frierson, 2013; Ceppi et al., 2013) and global cloud feedbacks (Gettelman et al., 2019; Zelinka et al., 2020). The fraction of sunlight reflected back to space (i.e. cloud albedo) depends strongly on the cloud microphysical properties (D. T. McCoy et al., 2014). In particular, the cloud droplet number concentration ($\mathrm{N_d}$) is a primary determinant of cloud albedo (Twomey et al., 1977; Merikanto et al., 2010; Diamond et al., 2020), a key variable that links aerosol and cloud microphysical properties (Boucher et al., 1995; Lohmann & Feichter, 2005), and also influences cloud macrophysical properties such as cloud depth, and cloud cover (Grosvenor et al., 2017; Christensen et al., 2020). Thus, a deeper understanding of the key controls on $\mathrm{N_d}$ is essential for understanding the climate effect of SO low clouds.

In liquid phase clouds, $\mathrm{N_d}$ is largely controlled by the balance between available aerosols in the boundary layer (BL) that serve as cloud condensation nuclei (CCN) and the loss of available CCN through the subsequent collision-coalescence of cloud droplets, which leads to precipitation and reduction of aerosol concentration. The removal of aerosols by their activation into cloud droplets and subsequent merger into precipitation-sized particles through collision-coalescence, hereafter coalescence scavenging, has long been recognized as a leading (if not the dominant) mechanism by which aerosols are removed from the BL (Feingold et al., 1996; Wood et al., 2012). This includes over the SO where aircraft observations have shown that aerosols that serve as CCN have lower concentrations in the BL under cloudy conditions than clear conditions (Hudson et al., 1998; Yum & Hudson, 2004).

Satellite observations show that SO low clouds have significant seasonal and latitudinal dependencies. Low clouds have higher mean $\mathrm{N_d}$ during the austral summer than winter, as well as higher mean $\mathrm{N_d}$ as one approaches Antarctica (south of 55° to 60° S) (D. T. McCoy et al., 2014; I. L. McCoy et al. 2020). Previous studies show that the seasonal and spatial patterns of SO $\mathrm{N_d}$ are strongly influenced by aerosol sources and coalescence scavenging. Using a source-and-sink budget model (Wood et al., 2012, hereafter W12), in combination with CloudSat-derived precipitation estimates, I. L. McCoy et al. (2020) found that the observed latitudinal gradient in SO $\mathrm{N_d}$ can be reasonably explained by increases in coalescence scavenging in low clouds associated with the storm track. Specifically, I. L. McCoy et al. (2020) suggest that coalescence scavenging may drive down mean N_{d} to about 30% of the value that would occur without coalescence scavenging over the storm track, while poleward of the storm track (65°S), its influence is weaker, perhaps reducing N_{d} to only about 70% of the value that would occur without this sink.

However, differences in aerosol sources compete with precipitation sink patterns in explaining the latitudinal dependence. Sources contribute heavily to seasonal differences, with ocean biology-sourced aerosols dominating CCN in the summertime and sea spray dominating in the winter (Ayers & Gras, 1991; Quinn et al., 2017). Observations and model studies (e.g., Korhonen et al., 2008) suggest that surface dimethyl sulfide (DMS) emissions associated with phytoplankton can be transported from the surface to the free troposphere (FT) where DMS oxidation products nucleate into new particles (Clarke et al., 1998; Weber et al., 2001). These particles subsequently return to the BL through entrainment and subsidence associated with mid-latitude storm systems (Covert et al. 1996) and grow into CCN (Raes, 1995; Quinn et al., 2017; Sanchez et al., 2021). I. L. McCoy et al. (2021) suggest that these FT Aitken particles (diameters 0.1 m), in addition to acting as the primary source of CCN, also buffer SO CCN and $\mathrm{N_d}$ against precipitation removal during biologically active time periods. The latitudinal pattern is driven in part by the large increases in the amount of phytoplankton and thus DMS production in the summertime seasonal ice zone around Antarctica (Curran & Jones, 2000) and increases in small aerosol particles south of the oceanic polar front during the SO summer (Humphries et al., 2016, 2021). Across the SO, strong correlations are observed between satellite retrieved $\mathrm{N_d}$ and sea surface chlorophyll-a concentrations (a proxy for phytoplankton biomass) (D. T. McCoy et al., 2015). Summertime BL accumulation mode aerosols (include most CCN) observed during the recent Southern Ocean Clouds Radiation Aerosol Transport Experimental Study (SOCRATES; McFarquhar et al., 2021) were dominated by sulfur-based particles (~70% by number) which likely had a biogenic origin. Sea-spray particles also contributed to the total (~30% by number) but many of these particles (40%) were still influenced by ocean biology as their compositions were salt enriched by sulfur and depleted in chlorine through uptake and condensation of sulfur gases (Twohy et al., 2020).

There is little doubt that aerosols from biological sources play a large role in both the seasonal and latitudinal variations in SO low cloud $\mathrm{N_d}$. However, coalescence scavenging has a non-trivial influence in determining the pattern of $\mathrm{N_d}$ across the SO, since it is the dominant sink of CCN, and its influence over the SO remains poorly understood. In this study, we examine this through a $\mathrm{N_d}$ budget model framework. We first test the ability of the W12 budget model to predict $\mathrm{N_d}$ for SO stratocumulus using SOCRATES observations. This model was developed in the context of observations gathered in subtropical stratocumulus and has been applied in other subtropical settings (Mohrmann et al., 2018; Zheng et al., 2018). While it was applied by I. L. McCoy et al. (2020) to the SO, it has not been tested in any detail at mid-to-high latitudes of either hemisphere. We find that the model (after being adjusted to better represent SO sea spray aerosols) can predict much of the observed N_d variability (section 3.1). This model skill is apparent in both regimes of liquid and mixed-phase precipitation (section 3.2), suggesting coalescence scavenging is a dominant sink for CCN. We then use the model to examine the relative importance of FT and surface sources of CCN and, to assess the importance of coalescence scavenging in controlling SO stratocumulus N_d (section 3.3).

2 Data and Methods

To quantitatively study the sources and sinks that control N_d, we apply a budget model, developed by W12, that considers the main sources and sinks of CCN and thus N_d:

$$\frac{\partial N}{\partial t} = \frac{\partial N}{\partial t}\Big|_{\mathrm{FT}} + \frac{\partial N}{\partial t}\Big|_{\mathrm{SFC}} + \frac{\partial N}{\partial t}\Big|_{\mathrm{New}} + \frac{\partial N}{\partial t}\Big|_{\mathrm{PRECIP}} + \frac{\partial N}{\partial t}\Big|_{\mathrm{DRY}} + \frac{\partial N}{\partial t}\Big|_{\mathrm{ADV}} \quad (1)$$

The terms on the right-hand side refer to the time tendency of CCN due to entrainment from the FT, primary production at the sea surface from sea-spray, new particle formation in BL, precipitation sink, dry deposition, and advection, respectively. For simplicity, W12 neglected terms for dry deposition ($\frac{\partial N}{\partial t}|_{\mathrm{DRY}}$), advection ($\frac{\partial N}{\partial t}|_{\mathrm{ADV}}$) and BL new particle formation ($\frac{\partial N}{\partial t}|_{\mathrm{New}}$) with the expectation that these terms are small on average over the ocean. The remaining terms for the FT source, surface source, and precipitation sink were parameterized. W12 derived a steady-state (or equilibrium solution) as N_{eq} for cloud droplet number concentration by setting the time tendency of CCN to zero (i.e. left-hand side of equation 1) and substituting in the parameterized source and sink terms:

$$N_{\mathrm{eq}} = \frac{(N_{\mathrm{FT}} + \frac{F(\sigma)U_{10}^{2.8}}{Dz_i})}{(1+\frac{\mathrm{hK}P_{\mathrm{CB}}}{Dz_i})} \quad (2)$$

where N_{FT} is the FT CCN concentration, z_i is the BL depth, D is the large-scale lower tropospheric divergence, $F(\sigma)$ is a sea spray source function that depends on the supersaturation (Clarke et al., 2006), U_{10} is the wind speed at 10 m, h is cloud thickness, P_{CB} is the precipitation rate at the cloud base and K is a constant that depends on the collection efficiency (Wood, 2006). Note that here we have modified the power-law relationship in the surface source parametrization from $U_{10}^{3.41}$ (as in W12) to $U_{10}^{2.8}$. Recent studies (Revell et al., 2019; Hartery et al., 2020) show that the previous $U_{10}^{3.41}$ parametrization (Monahan & Muircheartaigh, 1980; Gong, 2003; Clarke et al., 2006) can overestimate the surface source by a factor of 2-4 for the SO, while $U_{10}^{2.8}$ is a better fit for high-wind environments. Hartery et al. (2020) validated the new $U_{10}^{2.8}$ parametrization by comparing the predicted sea spray aerosol concentration with aircraft measurements during SOCRATES. In section 3, we will compare the budget model results using these two different parameterizations.

In this study, we test the budget model by using SOCRATES observations to calculate N_{eq} and compare it with the observed $\mathrm{N_d}$. Specifically, we estimate the model inputs (e.g., $\mathrm{N_{FT}}$, $\mathrm{P_{CB}}$, $\mathrm{U_{10}}$) from the aircraft measurements, as described below. During SOCRATES, typically, the Gulfstream-V aircraft flew south at high altitude, descended to just above cloud top before descending through the cloud, and then turning back toward Hobart. During the return flight, cloud and aerosol properties were sampled *in situ* using a standard flight module (Figure S1 is a schematic showing a typical flight module). The flight modules consisted of fixed activities such as ramp ascents and descents (sometimes called sawtooths), as well as ~10 minute above-, in-, and below-cloud legs flown at a constant altitude. Our analysis is focused on the below-cloud legs where the cloud-radar and lidar were pointing upward and could be used to assess precipitation. Specifically, we calculated N_{eq} based on the mean rain rate for the below-cloud legs and other supporting observations from surrounding legs (see Figure S1 for schematic), as described below, and obtained an associated estimate for observed $\mathrm{N_d}$ from cloud droplet probe (CDP) measurements taken in the adjacent in-cloud ramps.

For FT CCN concentration ($\mathrm{N_{FT}}$), we use measurements from the Ultra-High-Sensitivity Aerosol Spectrometer (UHSAS; DMT, 2013) during the nearby above-cloud leg. The UHSAS measures the size distribution and concentration of aerosols with diameters between 60 and 1000 nm. We calculated the concentration of aerosols with diameters larger than 70 nm and discarded 60-70 nm diameter range due to instrument noise (Sanchez et al., 2021). As discussed in Sanchez et al. (2021), the UHSAS concentration above 70 nm diameter have a strong equivalence to the CCN concentration at 0.3 % supersaturation.

For the surface source term, we use aircraft-measured wind speed from the below-cloud leg and extrapolate it to 10 m assuming a logarithmic wind profile (Hsu et al., 1994). A value of supersaturation $\sigma = 0.3\%$ is used, which yields a value for $F(\sigma)$ of 214 $\mathrm{m^{-3}}$ $(\mathrm{m\ s^{-1}})^{-(\mathrm{b}-1)}$ (where b is the wind speed exponent U_{10}^{b}) based on the parameterization of Clarke et al. (2006). We use 4 mm $\mathrm{s^{-1}}$ for the subsidence rate Dz_i, which is a typical value for low clouds in the subtropics and mid-latitudes, following I. L. McCoy et al. (2020).

For the precipitation sink term, the cloud thickness (h) is estimated from nearby sawtooth legs, where cloud top and cloud base are defined as the highest and lowest altitude with liquid water content > 0.03 g $\mathrm{m^{-3}}$, following Wood et al. (2011). In a few cases, multilayer clouds were present and the top and bottom were chosen to span over the levels that were consistent with the radar and lidar boundaries observed during the below cloud leg. We set $\mathrm{K} = 2.25\ \mathrm{m^2\ kg^{-1}}$, which is a constant that depends on the collection efficiency of cloud droplets by drizzle drops (Wood, 2006). We estimate the liquid precipitation rate at the cloud base (P_{CB}) based on the radar-lidar technique of O'Connor et al. (2005). This retrieval is run during the below-cloud legs when both the airbone W-band radar and high spectral resolution lidar (HSRL) were pointing upward, and only when the precipitation is identified as liquid phase. The precipitation phase is determined using HSRL measured particle linear depolarization ratio (PLDR) averaged over all levels below the cloud base. This measurement is taken below cloud base rather than at cloud base to prevent multiple scattering from significantly impacting the PLDR. Photons that are single-scattered from spherical droplets generate no PLDR. We interpret values of PLDR < 0.02 in each lidar column to be indicative of liquid precipitation, and PLDR > 0.05 to be ice, with PLDR values in between being mixed or ambiguous. In section 3.2, we define each below-cloud leg as a "liquid case" if 10% or less of the lidar columns have a PLDR > 0.05 or as a "mixed-phase case" otherwise.

We assess the fractional contribution of coalescence scavenging to $\mathrm{N_d}$ by computing the ratio between N_{eq} calculated with and without the precipitation sink, which is simply:

$$\frac{N_{\mathrm{eq}}(precip)}{N_{\mathrm{eq}}(no\ precip)} = \frac{1}{(1+\frac{\mathrm{hK}P_{\mathrm{CB}}}{Dz_i})} \qquad (3)$$

3 Results and Discussion

3.1 Evaluating the N_d Budget Model Accuracy

To quantify the accuracy of the budget model, we apply the model to *in situ* observations from SOCRATES flights as described in section 2. Figure 1a shows a comparison of observed $\mathrm{N_d}$ and model predicted equilibrium values ($\mathrm{N_{eq}}$) with all the source and sink terms and the adjusted wind speed parametrization as in equation (2). Each point represents a below-cloud leg sample that had sufficient supporting observations from surrounding legs for the model to be applied. (The aircraft-derived inputs for each sample are given in Table S1, with corresponding statistics also given in Table S2). Circular symbols are cases dominated by liquid precipitation while diamond-shaped symbols are mixed-phase cases (as determined from the lidar PLDR, see section 2). Implications of precipitation phase in the budget model results will be discussed in the next section.

Considering all cases together (Figure 1), we find the budget model performs remarkably well with a correlation coefficient of 0.72 (reported at 95% confidence here and throughout the study). Bias is also quite low, where observed $\mathrm{N_d}$ is 101 $\mathrm{cm^{-3}}$ while predicted $\mathrm{N_{eq}}$ is 106 $\mathrm{cm^{-3}}$. This level of performance with a low bias and a correlation coefficient ~0.7 is comparable to the performance of satellite retrievals for $\mathrm{N_d}$ (Kang et al., 2021). This confirms that the budget model, which has been previously applied over the sub-tropics (W12; Mohrmann et al., 2018; Zheng et al., 2018), can be used with confidence in the mid-latitudes once the wind speed parameterization in the surface term is appropriately adjusted. We will return to the topic of the wind speed and surface contribution to CCN in section 3.3.

3.2 *Sensitivity of the Budget Model to Precipitation Phase*

We hypothesize that CCN scavenging in SO clouds is dominated by liquid phase processes (i.e. coalescence scavenging). In general, ice precipitation that is driven by vapor deposition will not remove CCN from the atmosphere very efficiently (as one ice crystal may consume as little as one CCN particle if it grows exclusively by vapor deposition after a cloud droplet freezes) and it is only through riming, and to a lesser degree ice-aggregation, that ice precipitation might be expected to contribute significantly to CCN removal (Baltensperger et al., 1999; Garret et al., 2010). Rimed ice was frequently observed during SOCRATES and in past SO experiments, and secondary ice production through rime-splintering appears to be a significant factor in generating ice precipitation in SO clouds (Huang et al., 2017; McFarquhar et al., 2021). While rime-scavenging has long been recognized for its impact on the chemical composition of snow (Mitchell & Lamb 1989) and in recent years on its possible role in controlling black carbon in the Arctic (Hegg et al., 2011; Flanner et al., 2012; Qi et al., 2017; Xu et al., 2019), there has been little, if any, attention paid to the effect of riming on the overall CCN budget in mixed-phase clouds.

To test our hypothesis, Figure 1a compares N_{eq} to observed N_d separately for mixed-phase cases (diamonds) and liquid-phase cases (circles). For mixed-phase cases, we use the retrieved precipitation ONLY from lidar and radar columns with liquid precipitation. Specifically, we do not retrieve the precipitation rate during periods when lidar PLDR indicates ice is present, but rather we assume that the coalescence scavenging rate in the columns with ice precipitation is the same as in nearby liquid columns. In the context of the budget model we simply assign to the ice-columns the mean precipitation rate retrieved for the liquid-columns. We have not adjusted the budget model to include a rime-scavenging component. In general, we find that the mixed-phase cases behave similarly to the liquid cases (Figure 1a, Table S2). For liquid cases, we find a correlation coefficient of 0.72 and little bias (mean N_{eq} of 97 vs. mean N_d of 96 cm^{-3}), while for mixed-phase cases we find a correlation coefficient of 0.7 and slightly more bias (mean N_{eq} of 126 vs. mean N_d of 113 cm^{-3}). Our phase comparison results imply that CCN scavenging in SO clouds is likely dominated by liquid phase coalescence scavenging and the influence of mixed-phase processes on scavenging is small, at least in low-altitude SO cloud.

3.3 Quantifying the Relative Importance of Sources and Sinks

How important is coalescence scavenging in controlling N_d? We can easily answer this question in the context of the budget model. If the precipitation sink is removed from the model (Figure 1b), the predicted N_{eq} increases substantially, with the mean N_{eq} of liquid cases jumping from 97 cm^{-3} (Figure 1a) to 133 cm^{-3} (Figure 1b). Figure 2 shows the ratio between N_{eq} calculated with and without coalescence scavenging (equation 3) as a function of precipitation rate at cloud base. For precipitation rates below about 0.001 mm h^{-1} there is no appreciable reduction in N_{eq}. In Figure 1, cases with a precipitation rate greater than 0.001 mm h^{-1} are marked with black hyphens. The clear symbols (with no hyphen) remain clustered near but below the one-to-one line in Figure 1b, suggesting that source terms may be a bit too weak. On the other hand, for cases with precipitation rates above 0.001 mm h^{-1}, there is a sharp reduction in N_{eq} such that when precipitation rates reach 0.1 mm h^{-1}, N_{eq} is reduced to about 10% of what it would have been without precipitation (Figure 2). This result demonstrates that light precipitation with rates < 0.1 mm h^{-1} significantly impacts CCN and N_d. The RF13 cases (pink points in Figure 1 and 2) provide an excellent demonstration of the importance of coalescence scavenging. Measurements during RF13 were collected across a Pocket of Open Cells (POC), that is a region of open-cell or broken stratocumulus surrounded by closed-cell or overcast stratocumulus (see Figure S2). POCs are commonly observed in sub-tropical stratocumulus but also occur in SO stratocumulus. Measurement campaigns such as VOCALS have highlighted the importance of precipitation for forming and maintaining these structures (Berner et al., 2011). Not surprisingly, we find that SO POCs are also associated with increased precipitation and lower N_d. During RF13, samples in the closed cellular clouds had large values of N_d (up to ~160 cm^{-3}) while the two samples in the open cellular cloud regions had much lower values of N_d (~8 cm^{-3} and ~44 cm^{-3}), despite having very similar aerosols in the FT and similar surface winds.

What is the relative importance of the FT and surface sources of CCN? Again, we can examine this question in the context of the budget model by neglecting the source terms in estimating N_{eq}. Comparing Figure 1c (no FT source) and Figure 1d (no surface source) suggests that entrainment of FT CCN is playing a larger role than surface sources in controlling N_d on average during SOCRATES. For liquid cases, when removing surface sources (Figure 1d) the mean predicted N_{eq} drops from 97 to 74 cm^{-3}, while removing FT sources (Figure 1c) reduces N_{eq} to 23 cm^{-3}. This broadly matches the dominance of sulfur-based accumulation mode aerosols over sea-spray aerosols in the BL during SOCRATES (Twohy et al., 2021). Of course, the relative importance of the surface source varies with wind. This is evident in Figure 1c where flights with higher wind speeds (e.g., RF05, RF08, RF12) have a non-negligible surface source contribution to N_{eq}. Nonetheless, our analysis suggests that the FT is a larger source of CCN than the surface over the SO in summer, which is consistent with previous findings that FT aerosol is the dominant source for CCN in this part of the SO (Raes, 1995; Covert et al., 1996; Quinn et al., 2017). This differs, however, from the SO result in W12 where the budget model was originally introduced. W12 estimated the ratio of the CCN flux from the surface source to that from the FT and found that in the subtropics and tropics CCN was dominated by the FT source, but the mid-latitudes (including the SO), where winds are stronger, CCN was instead dominated by the surface source. The discrepancy between our analysis and W12 is due to the difference in the surface source parametrization. As noted in section 2, we have modified the power-law relationship in the surface source parametrization to one that is better suited to the SO. If we use the original budget model (W12) for SOCRATES cases, the predicted N_{eq} is overestimated (Figure S3), with the mean N_{eq} (223 cm^{-3}) of all cases more than twice of the observed mean N_d (101 cm^{-3}). This significant bias is caused by the high wind cases when using the original parameterization, as can be seen by examining the difference between N_{eq} and N_d as a function of wind speed (Figure S4). This highlights the importance of using a good parameterization for the surface source of CCN in the budget model and supports the $U_{10}^{2.8}$ relationship obtained by Revell et al. (2019) and Hartery et al. (2020) for the SO.

We also tested the performance of the budget model by using different input data for the surface wind speed and the precipitation rates. Specifically, we used ERA5 wind speed at 10 m ($U10_{ERA\text{-}5}$) as input, keeping all other inputs the same, and found the predicted N_{eq} still showed good agreement with observed N_d (Figure S5a). $U10_{ERA\text{-}5}$ is highly correlated with the U10 derived from aircraft measurements with a correlation coefficient of 0.96 and little bias (mean $U10_{ERA\text{-}5}$ of 10.2 m s^{-1} vs. mean $U10_{airfract}$ of 9.5 m s^{-1}). To examine the sensitivity of the budget model to precipitation rate estimates, we instead used a cloud-base precipitation rate estimated from a radar reflectivity to rain rate (Z-R) relationship developed by Comstock et al. (2004). For liquid cases, the predicted N_{eq} shows good agreement with observed N_d (Figure S5b). We note that for liquid cases the Comstock Z-R relationship was developed for subtropical clouds but compares reasonably well with our radar-lidar retrieval-based rain rate estimate (Figure S6).

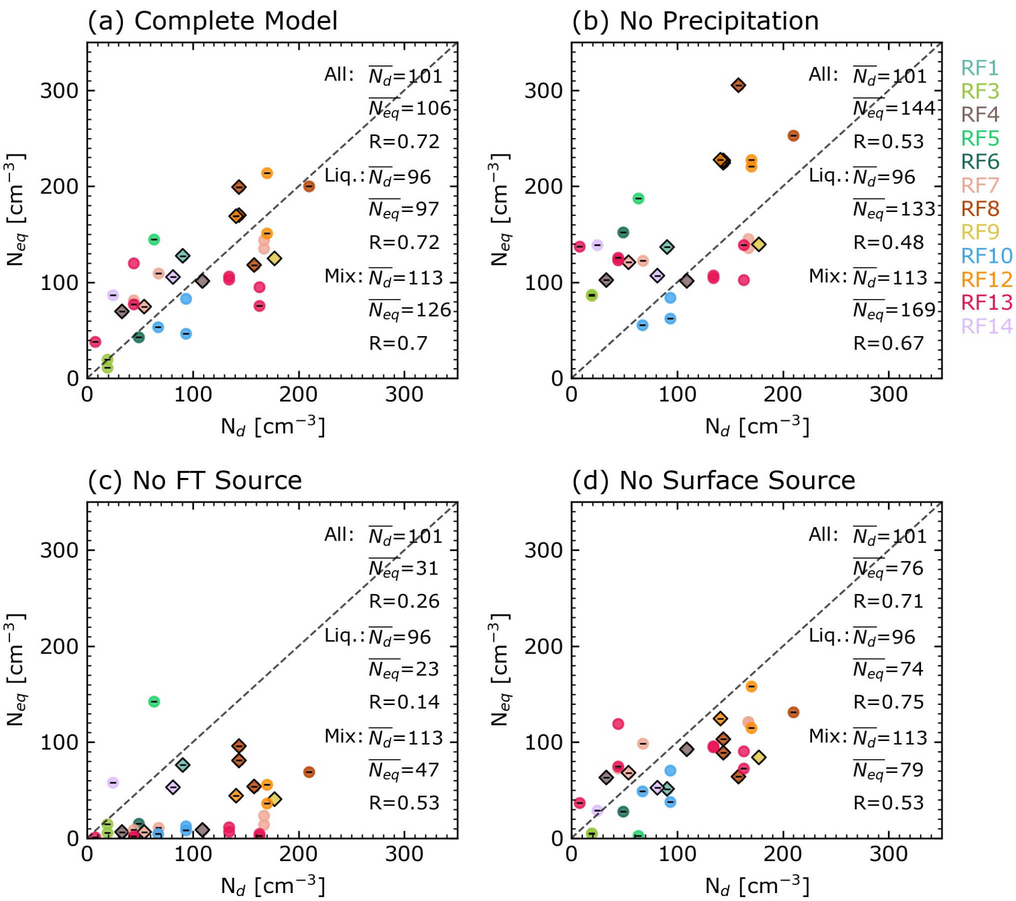

Figure 1. Comparison between observed N_d and computed N_{eq} using the budget model (equation 2) for SOCRATES flights: (a) with all the source and sink terms, (b) without the precipitation sink, (c) without the free tropospheric source, and (d) without the surface source. Different colors represent different flights. Circular points are cases associated with liquid precipitation. Black diamonds are the cases associated with mixed-phase precipitation, and, for these cases, the mean retrieved rain rates from the liquid-columns is used for the ice-columns. Black hyphens marked the cases with mean rain rate > 0.001 mm h^{-1}.

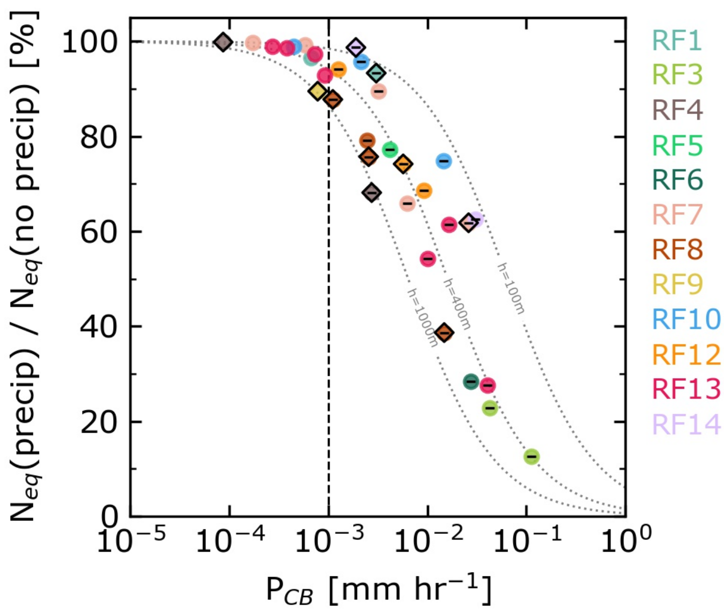

Figure 2. The ratio between calculated N_{eq} with and without the precipitation sink (equation 3) as a function of precipitation rate at cloud base. Different colors represent different flights. Black hyphens marked the cases with rain rate > 0.001 mm h^{-1} (which are to the right of the dashed reference line). Circular points are cases associated with liquid precipitation. Black diamonds are the cases associated with ice precipitation, and, for these cases, retrieved rain rates from liquid columns are used in the budget model. Grey dotted lines are the reference lines calculated using equation 3 assuming cloud depth h=100, 400, 1000 m.

4 Conclusions

In this study, we present an evaluation of the simple source-and-sink budget model developed in W12 by testing its accuracy with aircraft-based observations during the SOCRATES. The aircraft observations are used to estimate inputs to the budget model: the FT CCN concentration, near-surface wind speed, and cloud-base precipitation rate. We find that the budget model, after the CCN source term is adjusted to better represent SO sea spray aerosols, predicts SO N_d with little bias and a correlation coefficient of about 0.7 (Figure 1).

SOCRATES flights sampled in regimes where liquid-only and mixed-phase precipitation were present. We find that the budget model, when using only the liquid contribution to the precipitation rate (to estimate the coalescence scavenging rate), is able to predict N_d for both liquid and mixed-phase cases. This suggests that rime scavenging may not be very important to the SO CCN budget. However, it is important to recall that the SOCRATES data is a small sample of cases that are potentially biased towards cases with less riming. This is due to the experimental setup: sampling took place in the summer, with less ice presence (Danker et al., 2021), and the aircraft actively avoided stratocumulus with large amounts of supercooled liquid drizzle for safety. Thus, further investigation on the importance of rime scavenging seems warranted.

The only sink of CCN included in the budget model is coalescence scavenging, which we find reduces the predicted N_d by as much as 90% depending on the precipitation rate (Figure 2). This highlights the importance of coalescence scavenging in controlling CCN and N_d. In particular, the results demonstrate that light precipitation with rates < 0.1 mm h^{-1} significantly impacts CCN number. Such light precipitation is commonplace in SO stratocumulus but these rates are not captured well in current CloudSat W-band radar retrievals (Tansey et al., 2021), making it difficult to derive scavenging rates with CloudSat. This furthur suggests the impact of coalescence scavenging could be larger than the previous estimates based on CloudSat retrievals (I. L. McCoy et al., 2020). In climate models, as well, light precipitation remains poorly (typically over) simulated (e.g., Stephens et al., 2010; Zhou et al., 2020), and is known to have a disproportionately large effect on the aerosols (Wang et al., 2021). How well climate models simulate coalescence scavenging over the SO is an open question, and continued and improved observations of aerosol, cloud and precipitation properties over the SO is needed.

Regarding aerosol sources, we find that overall entrainment of FT CCN plays a larger role than surface sources in controlling N_d during SOCRATES. It should be stressed that SO CCN concentrations are much higher in summer (when SOCRATES was held) associated with increased emissions from ocean biology compared to winter (e.g., Ayers & Gras, 1991). This mostly influences the FT CCN source in the budget model as particles are generated from biological emissions above cloud and brought into the BL where they act as the key CCN source (e.g., Raes, 1995). During SOCRATES, the surface contribution is non-negligible for cases associated with high wind speeds. This could reflect increased production of sea spray particles from wind-driven processes (e.g., Grythe et al., 2014), increased fluxes of biological gases that help to grow already present particles to CCN sizes (e.g., Bates et al., 1998), or even an increased entrainment of FT Aitken particles to grow into CCN (e.g., Ayers et al., 1997). Budget model overestimation of N_d for these high-wind speed cases was reduced by modifying the surface source parametrization to a more appropriate SO representation. This, as in the global climate model study by Revell et al. (2019), highlights the importance of using a region appropriate parametrization for wind-speed driven surface CCN sources. If this budget model is to be applied widely, a more generalized parameterization may need to be implemented.

Lastly, while the source-sink framework shows skill in capturing observed SO N_d variability, there is still room for improvement. One likely source of remaining error is the parameterization of CCN entrainment into the BL. This is currently based on the large-scale divergence and was set to a fixed value. Variability in entrainment may be responsible for much of the remaining discrepancies between observed and predicted N_d. Likewise, new particle formation and the role of Aitken mode particles in buffering against precipitation removal of N_d and CCN (e.g., I. L. McCoy et al., 2021) is not included in the model. In our view, more detailed examinations of these factors, through large-eddy scale simulations of SOCRATES cases, should be undertaken.

Acknowledgments, Samples, and Data

This work was supported by the U.S. National Science Foundation on grants AGS-1660609 and AGS-2124993. Research by ILM is supported by the NOAA Climate and Global Change Postdoctoral Fellowship Program, administered by UCAR's Cooperative Programs for the Advancement of Earth System Science (CPAESS) under award NA18NWS4620043B.

We would like to thank the contribution from the many individuals and teams associated with the NCAR Earth Observing Laboratory, SOCRATES Science and Aircraft Instrument Teams. We also acknowledge the SOCRATES Project for providing datasets, including: low rate flight-level data (https://doi.org/10.5065/D6M32TM9), 2DS data (https://doi.org/10.26023/8HMG-WQP3-XA0X), and NCAR Cloud Radar and High Spectral Resolution Lidar moments (https://doi.org/10.5065/D64J0CZS).

References

Ayers, G. P., & Gras, J. L. (1991). Seasonal relationship between cloud condensation nuclei and aerosol methanesulphonate in marine air. *Nature*, *353*(6347), 834–835. https://doi.org/10.1038/353834a0

Ayres, G. P., Cainey, J. M., Gillett, R. W., & Ivey, J. P. (1997). Atmospheric sulphur and cloud condensation nuclei in marine air in the Southern Hemisphere. *Philosophical Transactions of the Royal Society B: Biological Sciences*, *352*(1350), 203–211. https://doi.org/10.1098/rstb.1997.0015

Baltensperger, U., Schwikowski, M., Jost, D. T., Nyeki, S., Gäggeler, H. W., & Poulida, O. (1998). Scavenging of atmospheric constituents in mixed phase clouds at the high-alpine site jungfraujoch part I: Basic concept and aerosol scavenging by clouds. *Atmospheric Environment*, *32*(23), 3975–3983. https://doi.org/10.1016/S1352-2310(98)00051-X

Bates, T. S., Kapustin, V. N., Quinn, P. K., Covert, D. S., Coffman, D. J., Mari, C., et al. (1998). Processes controlling the distribution of aerosol particles in the lower marine boundary layer during the First Aerosol Characterization Experiment (ACE 1). *Journal of Geophysical Research: Atmospheres*, *103*(D13), 16369–16383. https://doi.org/10.1029/97JD03720

Berner, A. H., Bretherton, C. S., & Wood, R. (2011). Large-eddy simulation of mesoscale dynamics and entrainment around a pocket of open cells observed in VOCALS-REx RF06. *Atmospheric Chemistry and Physics*, *11*(20), 10525–10540. https://doi.org/10.5194/acp-11-10525-2011

Boucher, O., & Lohmann, U. (1995). The sulfate-CCN-cloud albedo effect. *Tellus B: Chemical and Physical Meteorology*, *47*(3), 281–300. https://doi.org/10.3402/tellusb.v47i3.16048

Ceppi, P., Hwang, Y.-T., Liu, X., Frierson, D. M. W., & Hartmann, D. L. (2013). The relationship between the ITCZ and the Southern Hemispheric eddy-driven jet. *Journal of Geophysical Research: Atmospheres*, *118*(11), 5136–5146. https://doi.org/10.1002/jgrd.50461

Christensen, M. W., Jones, W. K., & Stier, P. (2020). Aerosols enhance cloud lifetime and brightness along the stratus-to-cumulus transition. *Proceedings of the National Academy of Sciences*, *117*(30), 17591–17598. https://doi.org/10.1073/pnas.1921231117

Clarke, A. D., Varner, J. L., Eisele, F., Mauldin, R. L., Tanner, D., & Litchy, M. (1998). Particle production in the remote marine atmosphere: Cloud outflow and subsidence during ACE 1. *Journal of Geophysical Research: Atmospheres*, *103*(D13), 16397–16409. https://doi.org/10.1029/97JD02987

Clarke, Antony D., Owens, S. R., & Zhou, J. (2006). An ultrafine sea-salt flux from breaking waves: Implications for cloud condensation nuclei in the remote marine atmosphere. *Journal of Geophysical Research: Atmospheres*, *111*(D6). https://doi.org/10.1029/2005JD006565

Comstock, K. K., Wood, R., Yuter, S. E., & Bretherton, C. S. (2004). Reflectivity and rain rate in and below drizzling stratocumulus. *Quarterly Journal of the Royal Meteorological Society*, *130*(603), 2891–2918. https://doi.org/10.1256/qj.03.187

Covert, D. S., Kapustin, V. N., Bates, T. S., & Quinn, P. K. (1996). Physical properties of marine boundary layer aerosol particles of the mid-Pacific in relation to sources and meteorological transport. *Journal of Geophysical Research: Atmospheres*, *101*(D3), 6919–6930. https://doi.org/10.1029/95JD03068

Curran, M. A. J., & Jones, G. B. (2000). Dimethyl sulfide in the Southern Ocean: Seasonality and flux. *Journal of Geophysical Research: Atmospheres*, *105*(D16), 20451–20459. https://doi.org/10.1029/2000JD900176

Danker, J., Sourdeval, O., McCoy, I. L., Wood, R., & Possner, A. (2021). Exploring Relations between Cloud Morphology, Cloud Phase, and Cloud Radiative Properties in Southern Ocean Stratocumulus Clouds. *Atmospheric Chemistry and Physics Discussions*, 1–26. https://doi.org/10.5194/acp-2021-926

Diamond, M. S., Director, H. M., Eastman, R., Possner, A., & Wood, R. (2020). Substantial Cloud Brightening From Shipping in Subtropical Low Clouds. *AGU Advances*, *1*(1), e2019AV000111. https://doi.org/10.1029/2019AV000111

DMT: Ultra High Sensitivity Aerosol Spectrometer (UHSAS) Operator Manual, Boulder, CO, 2013.

Feingold, G., Kreidenweis, S. M., Stevens, B., & Cotton, W. R. (1996). Numerical simulations of stratocumulus processing of cloud condensation nuclei through collision-coalescence. *Journal of Geophysical Research: Atmospheres*, *101*(D16), 21391–21402. https://doi.org/10.1029/96JD01552

Flanner, M. G., Liu, X., Zhou, C., Penner, J. E., & Jiao, C. (2012). Enhanced solar energy absorption by internally-mixed black carbon in snow grains. *Atmospheric Chemistry and Physics*, *12*(10), 4699–4721. https://doi.org/10.5194/acp-12-4699-2012

Garrett, T., Zhao, C., & Novelli, P. (2010). Assessing the relative contributions of transport efficiency and scavenging to seasonal variability in Arctic aerosol. *Tellus B: Chemical and Physical Meteorology*, *62*(3), 190–196. https://doi.org/10.1111/j.1600-0889.2010.00453.x

Gettelman, A., Hannay, C., Bacmeister, J. T., Neale, R. B., Pendergrass, A. G., Danabasoglu, G., et al. (2019). High Climate Sensitivity in the Community Earth System Model Version 2 (CESM2). *Geophysical Research Letters*, *46*(14), 8329–8337. https://doi.org/10.1029/2019GL083978

Gong, S. L. (2003). A parameterization of sea-salt aerosol source function for sub- and super-micron particles. *Global Biogeochemical Cycles*, *17*(4). https://doi.org/10.1029/2003GB002079

Grosvenor, D. P., Field, P. R., Hill, A. A., & Shipway, B. J. (2017). The relative importance of macrophysical and cloud albedo changes for aerosol-induced radiative effects in closed-cell stratocumulus: insight from the modelling of a case study. *Atmospheric Chemistry and Physics*, *17*(8), 5155–5183. https://doi.org/10.5194/acp-17-5155-2017

Grythe, H., Ström, J., Krejci, R., Quinn, P., & Stohl, A. (2014). A review of sea-spray aerosol source functions using a large global set of sea salt aerosol concentration measurements. *Atmospheric Chemistry and Physics*, *14*(3), 1277–1297. https://doi.org/10.5194/acp-14-1277-2014

Hartery, S., Toohey, D., Revell, L., Sellegri, K., Kuma, P., Harvey, M., & McDonald, A. J. (2020). Constraining the Surface Flux of Sea Spray Particles From the Southern Ocean. *Journal of Geophysical Research: Atmospheres*, *125*(4), e2019JD032026. https://doi.org/10.1029/2019JD032026

Hegg, D. A., Clarke, A. D., Doherty, S. J., & Ström4, J. (2011). Measurements of black carbon aerosol washout ratio on Svalbard. *Tellus B: Chemical and Physical Meteorology*, *63*(5), 891–900. https://doi.org/10.1111/j.1600-0889.2011.00577.x

Hsu, S. A., Meindl, E. A., & Gilhousen, D. B. (1994). Determining the Power-Law Wind-Profile Exponent under Near-Neutral Stability Conditions at Sea. *Journal of Applied Meteorology and Climatology*, *33*(6), 757–765. https://doi.org/10.1175/1520-0450(1994)033%3c0757:DTPLWP%3e2.0.CO;2

Huang, Y., Chubb, T., Baumgardner, D., deHoog, M., Siems, S. T., & Manton, M. J. (2017). Evidence for secondary ice production in Southern Ocean open cellular convection. *Quarterly Journal of the Royal Meteorological Society*, *143*(704), 1685–1703. https://doi.org/10.1002/qj.3041

Huang, Y., Siems, S. T., Manton, M. J., Rosenfeld, D., Marchand, R., McFarquhar, G. M., & Protat, A. (2016). What is the Role of Sea Surface Temperature in Modulating Cloud and Precipitation Properties over the Southern Ocean? *Journal of Climate*, *29*(20), 7453–7476. https://doi.org/10.1175/JCLI-D-15-0768.1

Hudson, J. G., Xie, Y., & Yum, S. S. (1998). Vertical distributions of cloud condensation nuclei spectra over the summertime Southern Ocean. *Journal of Geophysical Research: Atmospheres*, *103*(D13), 16609–16624. https://doi.org/10.1029/97JD03438

Humphries, R. S., Klekociuk, A. R., Schofield, R., Keywood, M., Ward, J., & Wilson, S. R. (2016). Unexpectedly high ultrafine aerosol concentrations above East Antarctic sea ice. *Atmospheric Chemistry and Physics*, *16*(4), 2185–2206. https://doi.org/10.5194/acp-16-2185-2016

Humphries, Ruhi S., Keywood, M. D., Gribben, S., McRobert, I. M., Ward, J. P., Selleck, P., et al. (2021). Southern Ocean latitudinal gradients of cloud condensation nuclei. *Atmospheric Chemistry and Physics*, *21*(16), 12757–12782. https://doi.org/10.5194/acp-21-12757-2021

Hwang, Y.-T., & Frierson, D. M. W. (2013). Link between the double-Intertropical Convergence Zone problem and cloud biases over the Southern Ocean. *Proceedings of the National Academy of Sciences*, *110*(13), 4935–4940. https://doi.org/10.1073/pnas.1213302110

Kang, L., Marchand, R., & Smith, W. (2021). Evaluation of MODIS and Himawari-8 Low Clouds Retrievals Over the Southern Ocean With In Situ Measurements From the SOCRATES Campaign. *Earth and Space Science*, *8*(3), e2020EA001397. https://doi.org/10.1029/2020EA001397

Korhonen, H., Carslaw, K. S., Spracklen, D. V., Mann, G. W., & Woodhouse, M. T. (2008). Influence of oceanic dimethyl sulfide emissions on cloud condensation nuclei concentrations and seasonality over the remote Southern Hemisphere oceans: A global model study. *Journal of Geophysical Research: Atmospheres*, *113*(D15). https://doi.org/10.1029/2007JD009718

Lohmann, U., & Feichter, J. (2005). Global indirect aerosol effects: a review. *Atmospheric Chemistry and Physics*, *5*(3), 715–737. https://doi.org/10.5194/acp-5-715-2005

Mace, G. G. (2010). Cloud properties and radiative forcing over the maritime storm tracks of the Southern Ocean and North Atlantic derived from A-Train. *Journal of Geophysical Research: Atmospheres*, *115*(D10). https://doi.org/10.1029/2009JD012517

Mace, G. G., Benson, S., & Hu, Y. (2020). On the Frequency of Occurrence of the Ice Phase in Supercooled Southern Ocean Low Clouds Derived From CALIPSO and CloudSat. *Geophysical Research Letters*, *47*(14), e2020GL087554. https://doi.org/10.1029/2020GL087554

Mace, G. G., Zhang, Q., Vaughan, M., Marchand, R., Stephens, G., Trepte, C., & Winker, D. (2009). A description of hydrometeor layer occurrence statistics derived from the first year of merged Cloudsat and CALIPSO data. *Journal of Geophysical Research: Atmospheres*, *114*(D8). https://doi.org/10.1029/2007JD009755

McCoy, D. T., Burrows, S. M., Wood, R., Grosvenor, D. P., Elliott, S. M., Ma, P.-L., et al. (2015). Natural aerosols explain seasonal and spatial patterns of Southern Ocean cloud albedo. *Science Advances*. https://doi.org/10.1126/sciadv.1500157

McCoy, D. T., Hartmann, D. L., & Grosvenor, D. P. (2014). Observed Southern Ocean Cloud Properties and Shortwave Reflection. Part I: Calculation of SW Flux from Observed Cloud Properties. *Journal of Climate*, *27*(23), 8836–8857. https://doi.org/10.1175/JCLI-D-14-00287.1

McCoy, I. L., Bretherton, C. S., Wood, R., Twohy, C. H., Gettelman, A., Bardeen, C. G., & Toohey, D. W. (2021). Influences of Recent Particle Formation on Southern Ocean Aerosol Variability and Low Cloud Properties. *Journal of Geophysical Research: Atmospheres*, *126*(8), e2020JD033529. https://doi.org/10.1029/2020JD033529

McCoy, I. L., McCoy, D. T., Wood, R., Regayre, L., Watson-Parris, D., Grosvenor, D. P., et al. (2020). The hemispheric contrast in cloud microphysical properties constrains aerosol forcing. *Proceedings of the National Academy of Sciences*, *117*(32), 18998–19006. https://doi.org/10.1073/pnas.1922502117

McFarquhar, G. M., Bretherton, C. S., Marchand, R., Protat, A., DeMott, P. J., Alexander, S. P., et al. (2021). Observations of Clouds, Aerosols, Precipitation, and Surface Radiation over the Southern Ocean: An Overview of CAPRICORN, MARCUS, MICRE, and SOCRATES. *Bulletin of the American Meteorological Society*, *102*(4), E894–E928. https://doi.org/10.1175/BAMS-D-20-0132.1

Merikanto, J., Spracklen, D. V., Pringle, K. J., & Carslaw, K. S. (2010). Effects of boundary layer particle formation on cloud droplet number and changes in cloud albedo from 1850 to 2000. *Atmospheric Chemistry and Physics*, *10*(2), 695–705. https://doi.org/10.5194/acp-10-695-2010

Mitchell, D. L., & Lamb, D. (1989). Influence of riming on the chemical composition of snow in winter orographic storms. *Journal of Geophysical Research: Atmospheres*, *94*(D12), 14831–14840. https://doi.org/10.1029/JD094iD12p14831

Mohrmann, J., Wood, R., McGibbon, J., Eastman, R., & Luke, E. (2018). Drivers of Seasonal Variability in Marine Boundary Layer Aerosol Number Concentration Investigated Using a Steady State Approach. *Journal of Geophysical*

Research: Atmospheres, *123*(2), 1097–1112. https://doi.org/10.1002/2017JD027443

Monahan, E. C., & Muircheartaigh, I. (1980). Optimal Power-Law Description of Oceanic Whitecap Coverage Dependence on Wind Speed. *Journal of Physical Oceanography*, *10*(12), 2094–2099. https://doi.org/10.1175/1520-0485(1980)010%3c2094:OPLDOO%3e2.0.CO;2

O'Connor, E. J., Hogan, R. J., & Illingworth, A. J. (2005). Retrieving Stratocumulus Drizzle Parameters Using Doppler Radar and Lidar. *Journal of Applied Meteorology and Climatology*, *44*(1), 14–27. https://doi.org/10.1175/JAM-2181.1

Qi, L., Li, Q., Li, Y., & He, C. (2017). Factors controlling black carbon distribution in the Arctic. *Atmospheric Chemistry and Physics*, *17*(2), 1037–1059. https://doi.org/10.5194/acp-17-1037-2017

Quinn, P. K., Coffman, D. J., Johnson, J. E., Upchurch, L. M., & Bates, T. S. (2017). Small fraction of marine cloud condensation nuclei made up of sea spray aerosol. *Nature Geoscience*, *10*(9), 674–679. https://doi.org/10.1038/ngeo3003

Raes, F. (1995). Entrainment of free tropospheric aerosols as a regulating mechanism for cloud condensation nuclei in the remote marine boundary layer. *Journal of Geophysical Research: Atmospheres*, *100*(D2), 2893–2903. https://doi.org/10.1029/94JD02832

Revell, L. E., Kremser, S., Hartery, S., Harvey, M., Mulcahy, J. P., Williams, J., et al. (2019). The sensitivity of Southern Ocean aerosols and cloud microphysics to sea spray and sulfate aerosol production in the HadGEM3-GA7.1 chemistry–climate model. *Atmospheric Chemistry and Physics*, *19*(24), 15447–15466. https://doi.org/10.5194/acp-19-15447-2019

Sallée, J.-B., Shuckburgh, E., Bruneau, N., Meijers, A. J. S., Bracegirdle, T. J., Wang, Z., & Roy, T. (2013). Assessment of Southern Ocean water mass circulation and characteristics in CMIP5 models: Historical bias and forcing response. *Journal of Geophysical Research: Oceans*, *118*(4), 1830–1844. https://doi.org/10.1002/jgrc.20135

Sanchez, K. J., Roberts, G. C., Saliba, G., Russell, L. M., Twohy, C., Reeves, J. M., et al. (2021). Measurement report: Cloud processes and the transport of biological emissions affect southern ocean particle and cloud condensation nuclei concentrations. *Atmospheric Chemistry and Physics*, *21*(5), 3427–3446. https://doi.org/10.5194/acp-21-3427-2021

Schneider, D. P., & Reusch, D. B. (2016). Antarctic and Southern Ocean Surface Temperatures in CMIP5 Models in the Context of the Surface Energy Budget. *Journal of Climate*, *29*(5), 1689–1716. https://doi.org/10.1175/JCLI-D-15-0429.1

Stephens, G. L., L'Ecuyer, T., Forbes, R., Gettelmen, A., Golaz, J.-C., Bodas-Salcedo, A., et al. (2010). Dreary state of precipitation in global models. *Jour-*

nal of Geophysical Research: Atmospheres, *115*(D24). https://doi.org/10.1029/2010JD014532

Tansey, E., Marchand, R., Protat, A., Alexander, S. P., Ding, S. (2021), Southern Ocean Precipitation Characteristics Observed from CloudSat and Ground Instrumentation during the Macquarie Island Cloud & Radiation Experiment (MICRE): April 2016 to March 2017. *Journal of Geophysical Research: Atmospheres*

Twohy, C. H., DeMott, P. J., Russell, L. M., Toohey, D. W., Rainwater, B., Geiss, R., et al. (2021). Cloud-Nucleating Particles Over the Southern Ocean in a Changing Climate. *Earth's Future*, *9*(3), e2020EF001673. https://doi.org/10.1029/2020EF001673

Twomey, S. (1977). The Influence of Pollution on the Shortwave Albedo of Clouds. *Journal of the Atmospheric Sciences*, *34*(7), 1149–1152. https://doi.org/10.1175/1520-0469(1977)034%3c1149:TIOPOT%3e2.0.CO;2

Wang, Y., Xia, W., Liu, X., Xie, S., Lin, W., Tang, Q., et al. (2021). Disproportionate control on aerosol burden by light rain. *Nature Geoscience*, *14*(2), 72–76. https://doi.org/10.1038/s41561-020-00675-z

Weber, R. J., Moore, K., Kapustin, V., Clarke, A., Mauldin, R. L., Kosciuch, E., et al. (2001). Nucleation in the equatorial Pacific during PEM-Tropics B: Enhanced boundary layer H2SO4 with no particle production. *Journal of Geophysical Research: Atmospheres*, *106*(D23), 32767–32776. https://doi.org/10.1029/2001JD900250

Wood, R., Bretherton, C. S., Leon, D., Clarke, A. D., Zuidema, P., Allen, G., & Coe, H. (2011). An aircraft case study of the spatial transition from closed to open mesoscale cellular convection over the Southeast Pacific. *Atmospheric Chemistry and Physics*, *11*(5), 2341–2370. https://doi.org/10.5194/acp-11-2341-2011

Wood, Robert, Leon, D., Lebsock, M., Snider, J., & Clarke, A. D. (2012). Precipitation driving of droplet concentration variability in marine low clouds. *Journal of Geophysical Research: Atmospheres*, *117*(D19). https://doi.org/10.1029/2012JD018305

Wood, Robert. (2006). Rate of loss of cloud droplets by coalescence in warm clouds. *Journal of Geophysical Research: Atmospheres*, *111*(D21). https://doi.org/10.1029/2006JD007553

Xu, J., Zhang, J., Liu, J., Yi, K., Xiang, S., Hu, X., et al. (2019). Influence of cloud microphysical processes on black carbon wet removal, global distributions, and radiative forcing. *Atmospheric Chemistry and Physics*, *19*(3), 1587–1603. https://doi.org/10.5194/acp-19-1587-2019

Yum, S. S., & Hudson, J. G. (2004). Wintertime/summertime contrasts of cloud condensation nuclei and cloud microphysics over the Southern Ocean. *Journal* *of Geophysical Research: Atmospheres*, *109*(D6). https://doi.org/10.1029/2003JD003864

Zelinka, M. D., Myers, T. A., McCoy, D. T., Po-Chedley, S., Caldwell, P. M., Ceppi, P., et al. (2020). Causes of Higher Climate Sensitivity in CMIP6 Models. *Geophysical Research Letters*, *47*(1), e2019GL085782. https://doi.org/10.1029/2019GL085782

Zheng, G., Wang, Y., Aiken, A. C., Gallo, F., Jensen, M. P., Kollias, P., et al. (2018). Marine boundary layer aerosol in the eastern North Atlantic: seasonal variations and key controlling processes. *Atmospheric Chemistry and Physics*, *18*(23), 17615–17635. https://doi.org/10.5194/acp-18-17615-2018

Zhou, X., Atlas, R., McCoy, I. L., Bretherton, C. S., Bardeen, C., Gettelman, A., et al. (2021). Evaluation of Cloud and Precipitation Simulations in CAM6 and AM4 Using Observations Over the Southern Ocean. *Earth and Space Science*, *8*(2), e2020EA001241. https://doi.org/10.1029/2020EA001241